BIOCHEMISTRY
including biophysical chemistry & molecular biology
Accelerated Publication

*Biochemistry* **2010,** *49,* 415–421 415
DOI: 10.1021/bi901995n

# Neutron Structure of Human Carbonic Anhydrase II: Implications for Proton Transfer[†]

S. Zoë Fisher,*[,‡] Andrey Y. Kovalevsky,[‡] John F. Domsic,[§] Marat Mustyakimov,[‡] Robert McKenna,[§] David N. Silverman,[∥] and Paul A. Langan[‡]

[‡]*Bioscience Division MS M888, Los Alamos National Laboratory, Los Alamos, New Mexico 87544,* [§]*Department of Biochemistry and Molecular Biology, P.O. Box 100245, University of Florida, Gainesville, Florida 32610, and* [∥]*Department of Pharmacology and Therapeutics, P.O. Box 100267, University of Florida, Gainesville, Florida 32610*

*Received November 19, 2009; Revised Manuscript Received December 18, 2009*

ABSTRACT: Human carbonic anhydrase II (HCA II) catalyzes the reversible hydration of carbon dioxide to form bicarbonate and a proton. Despite many high-resolution X-ray crystal structures, mutagenesis, and kinetic data, the structural details of the active site, especially the proton transfer pathway, are unclear. A large HCA II crystal was prepared at pH 9.0 and subjected to vapor H−D exchange to replace labile hydrogens with deuteriums. Neutron diffraction studies were conducted at the Protein Crystallography Station at Los Alamos National Laboratory. The structure to 2.0 Å resolution reveals several interesting active site features: (1) the Zn-bound solvent appearing to be predominantly a $D_2O$ molecule, (2) the orientation and hydrogen bonding pattern of solvent molecules in the active site cavity, (3) the side chain of His64 being unprotonated (neutral) and predominantly in an inward conformation pointing toward the zinc, and (4) the phenolic side chain of Tyr7 appearing to be unprotonated. The implications of these details are discussed, and a proposed mechanism for proton transfer is presented.

Human carbonic anhydrase II (HCA II) is an ~29 kDa monomeric metalloenzyme that uses a Zn hydroxide mechanism to catalyze the reversible hydration of $CO_2$ to $HCO_3^-$ and a proton. Catalysis by HCA II involves a two-step, ping-pong mechanism (eqs 1 and 2). The first step is the nucleophilic attack on $CO_2$ by a Zn-bound $OH^-$ to produce $HCO_3^-$. The product is displaced by a water molecule, and the second step requires a proton transfer event to regenerate the catalytic $OH^-$ from the Zn-bound $H_2O$. The symbol B in eq 2 represents a buffer in solution or an endogenous $H^+$ acceptor (*1*−*3*).

$$EZnOH^- + CO_2 \rightleftarrows EZnHCO_3^- \rightleftarrows EZnH_2O + HCO_3^- \quad (1)$$

$$EZnH_2O + B \rightleftarrows EZnOH^- + BH^+ \quad (2)$$

The details of substrate binding and conversion, as depicted in the first step, are fairly well understood, especially in light of recent reports of the crystal structure of the $CO_2$−HCA II catalytically productive complex (*4*, *5*). The structure reveals the binding mode of $CO_2$ in a side-on configuration but not coordinated to the zinc, in the hydrophobic pocket (Val121, Val143, Leu198, Val207, and Trp209) located behind the Zn-bound solvent (ZS). The binding of $CO_2$ displaces a solvent molecule, termed deep water (DW) because of its location. This DW is involved in a H-bond with the ZS in the absence of substrate (*6*, *7*). The rate of the $CO_2$ hydration step is near diffusion control ($10^8$ $M^{-1}$ $s^{-1}$). For $CO_2$ hydration, both $k_{cat}$ and $k_{cat}/K_M$ have pH profiles that are described by a single ionization with a p$K_a$ near 7 and increasing in activity as the pH increases (*1*).

The proton transfer step, the second stage of catalysis, is hypothesized to proceed via a hydrogen-bonded network of six water molecules that span an ~8−12 Å distance between the ZS and proton shuttle residue, His64. A number of studies have shown that His64 functions as a proton acceptor and donor in the shuttling pathway (*3*, *8*, *9*). Crystallographic studies have shown His64 observed in two distinct conformations, the inward conformation in which the imidazole is pointing toward the zinc and the outward conformation in which it points toward the exterior bulk solvent (*10*, *11*). The mechanism of transfer of protons through intervening water molecules to His64 is not clear; one possibility is via a Grotthuss mechanism with protons moving in a concerted manner through a hydrogen-bonded water chain (*12*). Other mechanisms involve the movement of the proton through a series of $H_5O_2^+$ (Zundel cation) and/or $H_9O_4^+$ (Eigen cation) configurations and emphasize the importance of electrostatics (*13*, *14*). A variety of plausible proton transfer pathways have been suggested (*15*).

There are several hydrophilic residues (Tyr7, Asn62, Asn67, Thr199, and Thr200) that line the active site of HCA II and interact with solvent molecules (*3*, *13*, *16*). Crystallographic studies of HCA II have identified several ordered water molecules in the active site, and their positions are conserved over a wide pH range (5.0−10.0) (*11*). Replacement of hydrophilic residues followed by structural and kinetic studies shows that disruption of the solvent positions can be correlated with changes in the rate of proton transfer in catalysis (*16*). Several high-resolution (to ~1 Å) X-ray structures of the wild type and mutants of

[†]The PCS is funded by the Office of Biological and Environmental Research of the Department of Energy. M.M. and P.A.L. were partly supported by a National Institute of General Medical Sciences-funded consortium (1R01GM071939-01) between Los Alamos National Laboratory and Lawrence Berkeley National Laboratory to develop computational tools for neutron protein crystallography. A.Y.K. was supported by LDRD Grant 20080789PRD3. This work was also partially funded by grants from the National Institutes of Health (GM25154 to D.N.S. and R.M.) and the Thomas Maren Foundation (R.M.).

*To whom correspondence should be addressed. E-mail: zfisher@lanl.gov. Telephone: (505) 665-4105. Fax: (505) 665-3024.


Published on Web 12/21/2009

HCA II have been reported; however, the protonation states of active site residues and the nature and hydrogen bonding orientations of the active site solvent have not been directly observed (*17*, *18*). In instances where H atoms were partially visible in the high-resolution X-ray data, the densities were ambiguous and therefore difficult to interpret. Despite the kinetic and structural data obtained for this enzyme over the last few decades, many issues related to hydrogen bonding and protonation states remain unclear. To address these questions, neutron diffraction studies of HCA II were initiated.

Unlike X-rays, neutrons diffract equally strongly from H, albeit negatively (scattering length of −3.7 fm), as from other atoms found in proteins (6.6 fm for C, 5.8 fm for O, 9.4 fm for N, and 2.8 fm for S), making the visualization and assignment of H atom positions feasible, even at medium resolution (*19*, *20*). Substitution of H with its isotope, D (scattering length of 6.7 fm), leads to an improvement in the coherent scattering (as H has a large negative scattering length and incoherent cross section) and facilitates the determination of D positions (*19*). In this way, neutron data can give important details regarding H−D exchange, orientations of solvent molecules, and protonation states of residues (*21*).

In electron density maps, water molecules usually appear as spherical peaks, indicating the position of the O atom. In contrast, the nuclear densities obtained for solvent through nuclear density maps appear extended, and these features are due to the strong scattering from one or two D atoms. X-ray and neutron diffraction data used together for model refinement are highly complementary and allow the accurate placement of O atoms and the subsequent refinement of the extended nuclear peaks as D atoms. This allows the accurate placement and orientation of $D_2O$ molecules, resulting in a detailed understanding of the hydrogen bonding, via the deuterium patterns, which can facilitate the elucidation of catalytic mechanisms (*22*, *23*).

A large, single, crystal of HCA II was prepared and allowed to undergo H−D vapor exchange for 2 months at room temperature (RT) to replace exchangeable protons with deuterons. Neutron diffraction data to 2.0 Å were collected at the Protein Crystallography Station at Los Alamos Neutron Science Center. An additional X-ray data set, from a crystal prepared under identical conditions, was also collected to enable a combined X-ray and neutron structure refinement (*21*). Several interesting active site features were observed in the neutron structure of HCA II: (1) the imidazole side chain of His64 being unprotonated/neutral and occupying a predominantly inward conformation, (2) the ZS appearing to be predominantly a $D_2O$ molecule, (3) the orientations of the solvent and their interactions being visible, and (4) the phenolic side chain of Tyr7 appearing to be unprotonated. The implications and possible importance of these observations for proton transfer in the catalytic mechanism are discussed. This is the first report of a neutron structure of a carbonic anhydrase.

## MATERIALS AND METHODS

*Crystallization*. Human carbonic anhydrase II was expressed, purified, and crystallized for neutron diffraction as described elsewhere (*24*). Briefly, after expression and purification, the enzyme was buffer exchanged into 100 mM Tris (pH 8.0) using a desalting column from GE Healthcare. The enzyme was concentrated to ∼15 mg/mL with an Amicon Ultra centrifugation filtration device with a molecular mass cutoff of 10 kDa. HCA II was crystallized at RT using the sandwich box setup from Hampton Research with nine-well glass plates. Each well consisted of 400 μL: 200 μL of the protein solution and 200 μL of crystallization solution [1.15 M sodium citrate and 100 mM Tris (pH 9.0)]. The crystallization drops were equilibrated against 30 mL of well solution [1.3 M sodium citrate and 100 mM Tris (pH 9.0)]. No crystal growth occurred within a week; accordingly, sodium citrate salt was added to the well solution to a final concentration of ∼1.6 M. The sodium citrate recrystallized in the well, indicating saturation. Useful HCA II crystals appeared within a week and grew to a maximum size within 2 weeks. All expression, purification, and crystallization procedures were performed using $H_2O$ as a solvent and in precipitant suspensions.

*Neutron and X-ray Data Collection and Processing*. Neutron and X-ray data collection were conducted as described previously (*24*). Briefly, a suitable crystal for neutron diffraction (volume of ∼1.2 $mm^3$) was mounted in a quartz capillary, with mother liquor plugs containing 99% $D_2O$ introduced prior to sealing. The crystal was then left to undergo H−D exchange by vapor diffusion at RT for at least 2 months prior to data collection. Time-of-flight neutron Laue data were collected at RT on the Protein Crystallography Station (Los Alamos Neutron Science Center) $He^3$-filled position sensitive detector, with the sample mounted on a Huber κ-circle goniometer (*25*). Forty-one settings were collected, with an approximately 32 h exposure per image, with maximum usable diffraction to ∼2 Å resolution. Table 1 shows the data set and refinement statistics. The images were processed with a modified version of *d*Trek* and wavelength normalized with LAUENORM (*26*, *27*). Finally, data were merged with SCALA from the CCP4 suite; all data collection and refinement statistics are given in Table 1 (*28*).

A crystal of similar dimensions from the same drop and subjected to the same H−D vapor exchange was used for RT X-ray data collection. Diffraction data to 1.5 Å resolution were recorded on a R-AXIS $IV^{++}$ image plate using a Rigaku HU-H3R Cu rotating anode, with oscillation steps of 0.5° and a 2 min exposure per frame. The crystal−detector distance was 80 mm. Data processing and reduction were conducted using HKL2000 (*29*). X-ray data set statistics are given in Table 1.

*Joint X-ray and Neutron Refinement*. Refinement of the model was conducted utilizing a version of CNS modified for neutron refinement, nCNS, and a starting model generated from Protein Data Bank (PDB) entry 2ili, a high-resolution structure crystallized using similar conditions (*18*, *21*, *30*). The model was initially refined against only the X-ray data using SHELXL, until the *R* factors converged (*31*). At this point, H atoms were included in the model, as were D atoms at labile positions. Then the refinement against both X-ray and neutron data was moved into nCNS and included rigid body refinement, followed by iterative rounds of positional, individual *B* factor, and occupancy refinement. Visual inspection of nuclear and electron density $2F_o - F_c$ and $F_o - F_c$ maps allowed for the placement of $D_2O$ molecules and identification of the protonation states of amino acid side chains. In cases where the neutron data were not clear, H or D atoms and solvent were oriented to accommodate H-bonds and electrostatic interactions. All manual model building was conducted using Coot, and figures were generated with PyMOL (*32*, *33*). Table 1 shows a summary of the refinement statistics.

X-ray data from an isomorphous crystal are required to provide a starting model and structure factors for the joint X-ray and neutron refinement, as this approach vastly improves the nuclear density maps (*21*). The final model, refined against both neutron and X-ray data sets, had $R_{cryst}$ values of 27.5 and 16.1% and $R_{free}$ values of 28.6 and 17.3%, respectively. The

Table 1: Data Collection and Refinement Statistics

| | X-ray | neutron |
|---|---|---|
| wavelength $\lambda$ source | 1.54 Cu $\kappa\alpha$ anode | 0.7−6.3 Spallation neutron source LANSCE |
| unit cell dimensions | $a$ = 42.6 Å, $b$ = 41.6 Å, $c$ = 72.8 Å, $\beta$ = 104.6° | |
| space group | $P2_1$ | |
| no. of settings | 1255 | 41 |
| resolution (Å) | 20.0−1.50 (1.55−1.50)[a] | 20.0−2.00 (2.11−2.00)[a] |
| no. of reflections | 959116 (38510)[a] | 14136 (1760)[a] |
| redundancy | 9.4 (8.6)[a] | 3.0 (2.0)[a] |
| completeness (%) | 95.9 (91.9)[a] | 84.6 (72.8)[a] |
| mean $I/\sigma(I)$ | 31.0 (5.7)[a] | 3.8 (1.6)[a] |
| $R_{sym}$[b] | 5.8 (30.8)[a] | 27.1 (38.4)[a] |
| $R_{pim}$[c] | not available | 17.1 (28.5)[a] |
| $R_{cryst}$[d]/$R_{free}$[e] | 16.1/17.3 | 27.5/28.6 |
| no. of protein atoms/no. of $D_2O$ molecules | | 4072 232 |
| average $B$ factor (main chain/side chain/$D_2O$) | | 21.5/24.2/38.7 |
| root-mean-square deviation for bond lengths (Å), angles (deg) | | 0.010, 1.793 |

[a]Values in parentheses are for the highest-resolution shell. [b]$R_{sym} = (\sum|I - \langle I\rangle|/\sum\langle I\rangle) \times 100$. [c]$R_{pim} = \{\sum[1/(N-1)]^{1/2}/\sum|I - \langle I\rangle|/\sum\sum I\} \times 100$. [d]$R_{cryst} = (\sum||F_o| - |F_c||/\sum|F_o|) \times 100$. [e]$R_{free}$ is calculated in the same way as $R_{cryst}$ for data omitted from refinement (5% of reflections for all data sets).

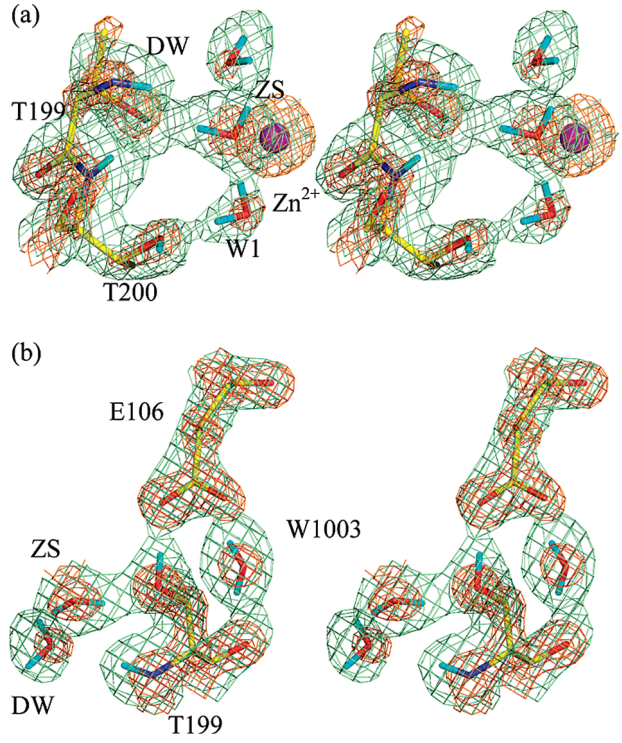


FIGURE 1: Stereoview of the catalytic Zn-bound solvent and interactions with Thr199. (a) H-Bonds between Zn-bound solvent (ZS), deep water (DW), and W1. (b) H-Bonded network between Thr199 and Glu106. D atoms are colored cyan; nuclear density maps are colored green and are contoured at 2.0$\sigma$, and electron density maps are colored orange and contoured at 4.0$\sigma$.

model contains 232 water molecules, modeled as $D_2O$, and has standard geometry with a root-mean-square deviations (rmsds) for bond lengths and angles of 0.01 Å and 1.8°, respectively. Model coordinates and experimental data have been deposited in the Protein Data Bank as entry 3KKX.

## RESULTS AND DISCUSSION

*Active Site Zn-Bound Solvent and Interactions*. From the shape of the nuclear density maps, the location of two deuteriums on the ZS is clearly visible. Thus, it appears that the ZS is present under these crystallization conditions as a zinc-bound $D_2O$ molecule (Figure 1a). This is the first direct observation showing the metal-bound solvent to be a water molecule in carbonic anhydrase. Even using atomic-resolution (~1 Å) macromolecular crystal structures, it is not possible to distinguish between Zn−$OH^-$ and Zn−$H_2O$ species, based on metal−oxygen distances alone. In both cases, the distances range from ~1.98 to 2.11 Å, and possibly the only way to distinguish these structurally is to look at high-resolution neutron diffraction data of small molecules (*34*). Another possibility is that we observe the ZS as an $OD^-$ bound in two orientations, one a H-bond donor to DW and the second a H-bond donor to Thr199, or even the superposition of a single $OD^-$ and $D_2O$. The p$K_a$ of zinc-bound water in HCA II in solution is well established as ~7.0 (*1*, *8*). Replacing exchangeable H with D could increase the p$K_a$ of zinc-bound $D_2O$ to around 7.5 if it behaves like a normal acid (*35*). Also, there is evidence that the p$K_a$ of the Co(II)-bound solvent is increased from 7.0 to 8.4 for crystals of Co(II)-substituted HCA II prepared in 1.4 M citrate (*36*). The starting crystallization pH in this study was ~9.0, and crystals were prepared in 1.15 M citrate, implying that the p$K_a$ of ZS could be higher than expected, leading to a $D_2O$ bound at the metal.

Attempts to model combinations of $OD^-$ in two orientations or superimposed with $D_2O$ led to unresolved $F_o - F_c$ nuclear density, and modeling a single $D_2O$ molecule provided the best fit to the observed data. Figure S1 of the Supporting Information shows an $F_o - F_c$ nuclear omit map generated with both D atoms on ZS removed, and this strongly suggests the presence of a $D_2O$ molecule. An occupancy refinement of just these two D atoms resulted in occupancies of 1.0 and 0.94, also supporting the assignment of a single $D_2O$ bound to the metal.

The ZS is a H-bond donor to the hydroxyl group of Thr199 with a H-bond distance of 2.9 Å (Figure 1b and Table 2). ZS is also a H-bond donor to DW and an acceptor from water molecule W1 (Figure 1a and Table 2). The O···O distances for the H-bonds between ZS and DW and W1 are both ~2.5 Å in these data at 1.5 Å resolution and could represent strong H-bonds (Table 2). This is consistent with the bond distances observed in an X-ray structure of HCA II at 0.9 Å resolution (*37*).

*Water Molecules and Interactions with Active Site Residues*. A network of water molecules extends from the ZS to the proton shuttle residue His64 in its inward orientation (Figures 2 and 3a). This network as observed in the crystal is a low-energy conformation of water molecules and provides important clues about the pathways of proton transfer during

Table 2: H-Bond Distances in the Active Site

| donor−acceptor[a] | O···O distance (Å) | D···O distance (Å) |
|---|---|---|
| ZS−DW | 2.5 | 1.7 |
| W1−ZS | 2.5 | 1.5 |
| W1−W2 | 2.8 | n/a |
| W2−W3a | 2.7 | 1.9 |
| W2−W3b | 2.8 | 1.8 |
| W1003−Glu106 | 2.8 | 1.9 |
| W1003−Thr199 | 2.8 | 1.9 |
| ZS−Thr199 | 2.9 | 1.9 |
| T199−Glu106 | 2.6 | 1.7 |
| W3a−Tyr7 | 2.9 | 2.0 |
| Tyr7−W1003 | 2.6 | n/a |

[a]Donor−acceptor groups for amino acids refer to the side chains only.

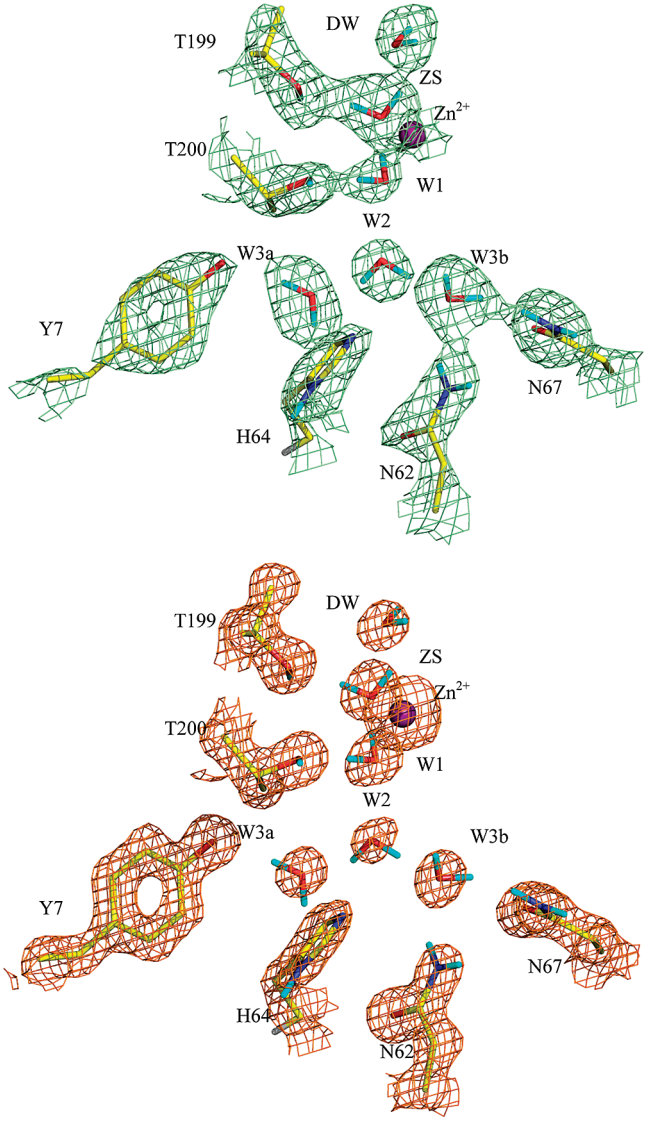


FIGURE 2: Water structure and its interactions with active site residues. Amino acid residues and solvent are as labeled. H-Bonding distances between the solvent and residues are listed in Table 2. D atoms are colored cyan. The $2F_o - F_c$ nuclear map is colored green (top panel) and is contoured at $1.5\sigma$. The $2F_o - F_c$ electron density is colored orange (bottom panel) and is contoured at $2.0\sigma$.

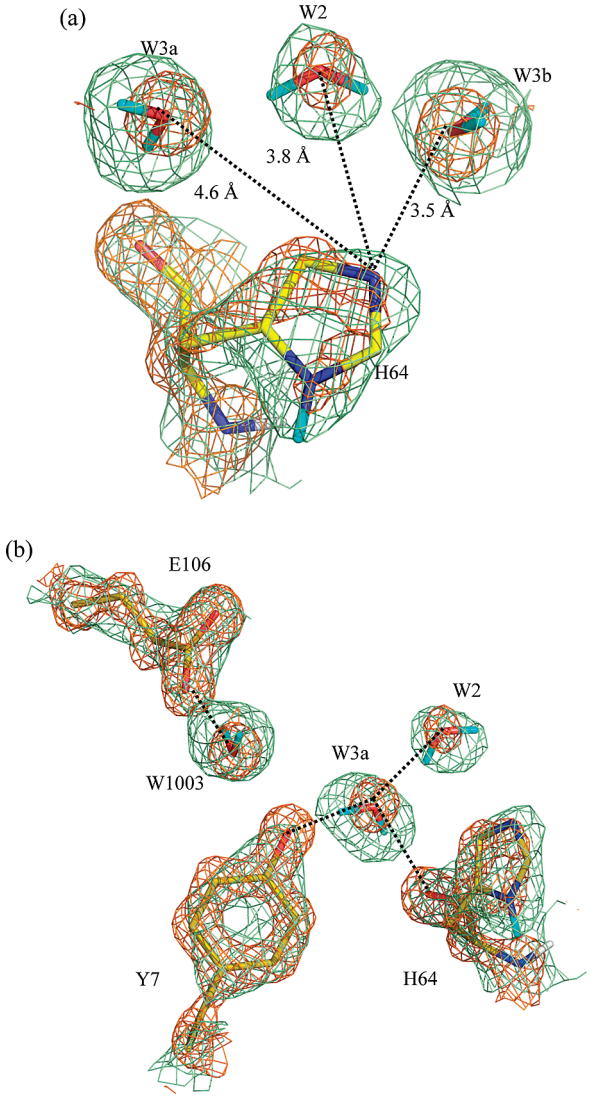


FIGURE 3: Orientation and charged state of His64 and Tyr7. (a) His64 is oriented completely in the inward conformation and is neutral with the exchanged D atom on ND1. The dashed lines indicate the N−O distances between His64 and the solvent. (b) Tyr7 appears to be deprotonated and is coordinated with W1003 and W3a. The dashed lines indicate H-bonds, and distances are listed in Table 2. D atoms are colored cyan. Positive $2F_o - F_c$ nuclear maps are colored green and are contoured at $1.5\sigma$; electron density maps are colored orange and are contoured at $2.5\sigma$.

catalysis. In solution, water clusters in the active site cavity form with a lifetime in the low picosecond range (*13*). Novel data provided by neutron diffraction are the orientations of H-bonds. The cluster of three water molecules (DW, ZS, and W1) is oriented such that DW and ZS are H-bond acceptors (Table 2). In a second cluster, water molecules W2, W3a, and W3b are H-bonded to each other with D atoms oriented toward but not directly H-bonded to His64 in its inward conformation (Figure 3a). There is no H-bond formed between W1 and W2 (Figure 2 and Table 2). In the crystal, there is no continuous, H-bonded water chain connecting ZS and the shuttle residue, His64. These are features that are also evident from the X-ray diffraction studies (*18*). Even though it is known that the O positions of the active site waters are conserved over a wide pH range, it is not known whether this is also the case for the H orientations and H-bond interactions in which they participate (*11*). It is very important to determine a neutron structure of wild-type HCA II at lower pH to determine how ionization and pH could affect the water orientations.

There is a cluster of H-bonds among the hydroxy group of Thr199, Glu106, and buried water W1003 (Figure 1b and Table 2). These interactions serve in part to orient the side chain of Thr199 toward ZS and likely help to stabilize the deprotonated ZS in an orientation to enhance catalysis (*38*).

The H-bond interactions between W3b and Asn62 and Asn67 can also be seen for the first time (Figure 2). The oxygen of W3b is H-bonded not only to one of the D atoms of W2 but also to the ND2 atom of the side chain of Asn62, while one of the D atoms interacts with the OD1 atom of the Asn67 side chain (Figure 2). W3a donates one of its D atoms to a H-bond with Tyr7 and the other to the backbone carbonyl of His64.

*Proton Shuttle His64*. Figure 3a shows the uncharged state and conformation of the imidazole side chain of the proton shuttle, His64. The side chain of His64 appears predominantly in the inward conformation, consistent with previous observations of the flexible side chain of His64 preferring an inward occupancy with an increase in pH (*10*, *11*). It is also clear from the nuclear density maps that His64 is neutral in this conformation (at this pH) and that the D atom located on the ND1 group is oriented away from the active site (Figure 3a). This supplements the observations made from the 1.05 Å resolution X-ray structure of HCA II. In that case, it was difficult to assign the H atom positions because His64 was occupying both the inward and outward conformations, making the densities ambiguous (*18*). However, with neutrons, the scattering from this D atom is very strong and the peak is easy to interpret, even at 2.0 Å resolution.

*Tyrosine 7*. An unexpected observation involves the phenol side chain of Tyr7. It appears that the phenolic oxygen of Tyr7 is primarily not protonated in the neutron crystal structure (Figure 3b). There is no D or H atom observed in either omit $F_o - F_c$ or negative $2F_o - F_c$ nuclear density maps. There are three possible explanations for this. (1) The phenolic D atom is present but is disordered, and the density for it is ill-defined. (2) The phenolic H atom is present (but not visible) because it did not exchange with a D in the vapor exchange with $D_2O$. (3) The residue is deprotonated at the high pD (9.0) of the crystal. Several arguments support option 3. First, Tyr7 and the surrounding residues appear very well ordered, with average *B* factors between 18 and 21 Å$^2$ (average for the whole protein of ~22 Å$^2$). Second, the residue is coordinated to two fully H−D exchanged $D_2O$ molecules, showing that this residue is exchangeable and solvent accessible (Table 2). Also, the aromatic H atoms are visible in negative $2F_o - F_c$ nuclear maps (Figure S2 of the Supporting Information), implying that we should be able to observe an H atom on the oxygen, if it was there. Third, low p$K_a$ values (p$K_a$ ~ 7−9) for Tyr residues have been reported in the literature. These are usually due to their proximity to a positively charged species such as Lys or Arg (*39*, *40*). This is not necessarily the case in HCA II, where Tyr7 is surrounded by Trp5, Trp16, His64, Thr200, Asn244, and Trp245 and is ~7 Å from the $Zn^{2+}$ center. Consequently, we conclude that the side chain of Tyr7 is not protonated in this study.

There is little support for the ionization of Tyr7 from accumulated research on HCA II. Possibly, an ionization event at Tyr7 would not be detected in pH profiles of catalysis of $CO_2$ hydration and ester hydrolysis, both of which fit well to single ionizations over the pH range from 6.0 to 10.0 (*1*). Additionally, pH profiles of anion and inhibitor binding might not have detected such ionization; the side chain of Tyr7 is 7 Å from the zinc, possibly too far to have an effect on these observations.

Whether an unprotonated Tyr at position 7 has any functional significance is uncertain. It is highly unlikely that this residue would ever be exposed to such an extreme pH environment in vivo. However, we know that HCA II supports proton transfer at high pH in vitro, and if this residue is indeed deprotonated due to pH, it may have an effect on how proton transfer proceeds under these conditions. It is reasonable to expect that a negatively charged species close to the water network could favor the formation, and stabilization, of an excess proton in the form of a Zundel cation.

*Proposed Mechanism of Proton Transfer*. The observed structure demonstrates an ordered water network of low energy, and although this structure is observed under conditions different from the solution conditions under which rates of proton transfer are measured, the structure gives important clues about proton transfer pathways occurring in catalysis. The ionization states of ZS and His64 are appropriate for proton transfer accompanying hydration; that is, ZS appears as $D_2O$ a proton donor and His64 neutral as an acceptor. However, the water network that is observed is not a continuously H-bonded chain, as noted above, and the orientations of H-bonds are not optimal for the transfer of protons from ZS to His64 (Figures 1a and 3a and Table 2). On the basis of the orientation of H-bonds in the cluster of DW, ZS, and W1, there would need to be a rearrangement of H-bonds to promote proton transfer during catalyzed hydration. A possible rearrangement is shown in the second panel of Scheme 1. This rearrangement would involve the breaking of the observed H-bonds between ZS-DW and ZS-W1, flipping of ZS and W1 with subsequent formation of new H-bonds in another orientation (Scheme 1). This might also involve a reorientation of DW. The reorientations would be expected to occur if the proton transfer is stepwise or concerted.

The next step of proton transfer includes formation of the zinc-bound $OH^-$ and possibly a Zundel-like cation ($H_5O_2^+$) formed with W1 and W2 (Scheme 1). The Zundel cation is a type of hydrated proton and a likely participant in the proton transfer pathway as found and thoroughly discussed in the computations of Maupin et al. (*13*). The observed structure does not show D atom density between W1 and W2, although the O−O distance is 2.8 Å; the flipping of W1 and subsequent motion of a proton from ZS to W1 would proceed to a Zundel cation (Scheme 1). The excess proton then proceeds through hydrated forms resembling Zundel or perhaps Eigen ($H_9O_4^+$) complexes to His64, with computations showing transfer proceeding through W3a (*13*). All of these events potentially represent energy barriers as the proton moves from ZS to His64. The breaking and re-formation of H-bonds and the rotation of the solvent molecules could contribute to the energy barrier near 10 kcal/mol associated with proton transfer in catalysis. Computational studies using multistate empirical valence bond methods compute a free energy barrier of 10 kcal/mol for the transfer of protons from ZS to His64 in the inward conformation (*13*).

The distances observed from the NE2 atom of His64 in the inward conformation to either W2, W3a, or W3b (Figure 3a) are too long to support proton transfer through a direct H-bond; however, there is considerable flexibility along $\chi_1$ and $\chi_2$ of the side chain of His64, and it could be hypothesized that His64 may move closer to these solvent molecules to form such a H-bond. Again, this is a potentially an energy barrier to proton transfer.

Scheme 1: Diagram Summarizing the Orientations of Hydrogen Bonds in the Ordered Water Structure Determined from Neutron Diffraction[a]

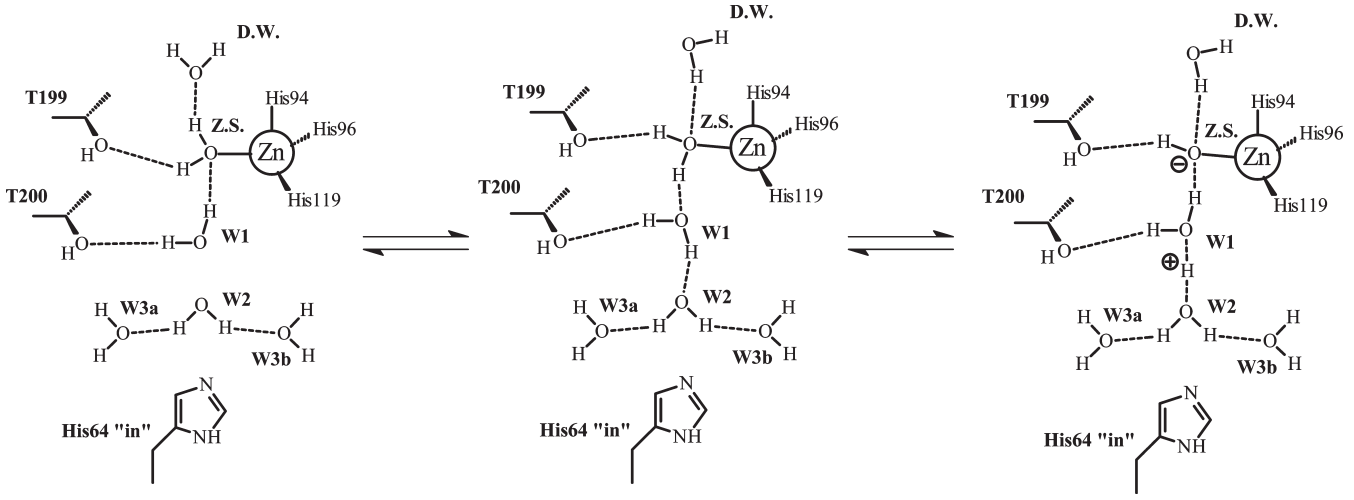


[a]Also shown is possible formation of a Zundel cation ($H_5O_2^+$) involving water molecules W1 and W2 in the ordered water structure as the excess proton moves from donor ZS to acceptor His64. The large sphere is the zinc ion.

## CONCLUSIONS

This is the first report of the neutron structure of any carbonic anhydrase, and the data elucidate interesting features of the active site not previously observed with implications for the proton transfer pathway during catalysis. The zinc-bound solvent appears to be $D_2O$ and is involved in two hydrogen bonds to DW and W1. The details of the side chain orientations of Thr199 and Glu106 are also visible, and these interact in a way that facilitates the orientation of the Zn-bound $OH^-$ in catalysis. The details of the ordered water structure that occupies the active site are also visible, and their orientations suggest that cleavage of H-bonds and flipping of water molecules are required for the excess proton to leave the active site during catalysis. The proton shuttle His64 is oriented predominantly in the inward conformation and is neutral, with the unprotonated NE2 atom pointing toward the zinc-bound $D_2O$, ready to pick up a proton. Finally, Tyr7 appears to be deprotonated at the crystallization pH of 9.0. The possible role of tyrosine deprotonation in the catalytic mechanism of HCA II, if any, remains to be elucidated.

## ACKNOWLEDGMENT

R.M. thanks Joseph Kalb (Gilboa) and Dean Myles for introducing him to the possibilities of neutron diffraction studies on HCA II.

## SUPPORTING INFORMATION AVAILABLE

Positive omit $F_o - F_c$ map for the Zn-bound solvent (Figure S1) and negative and positive $2F_o - F_c$ nuclear density maps for Tyr7 (Figure S2). This material is available free of charge via the Internet at http://pubs.acs.org.

## REFERENCES

1. Silverman, D. N., and Lindskog, S. (1988) The catalytic mechanism of carbonic anhydrase: Implications of a rate-limiting protolysis of water. *Acc. Chem. Res. 21*, 30–36.
2. Christianson, D. W., and Fierke, C. A. (1996) Carbonic anhydrase: Evolution of the zinc binding site by nature and by design. *Acc. Chem. Res. 29*, 331–339.
3. Silverman, D. N., and McKenna, R. (2007) Solvent mediated proton transfer in catalysis by carbonic anhydrase. *Acc. Chem. Res. 40*, 669–675.
4. Domsic, J. F., Avvaru, B. S., Kim, C. U., Gruner, S. M., Agbandje-McKenna, M., Silverman, D. N., and McKenna, R. (2008) Entrapment of carbon dioxide in the active site of carbonic anhydrase II. *J. Biol. Chem. 283*, 30766–30771.
5. Sjoblom, B., Polentarutti, M., and Djinovic-Carugo, K. (2009) Structural study of X-ray induced activation of carbonic anhydrase. *Proc. Natl. Acad. Sci. U.S.A. 106*, 10609–10613.
6. Hakansson, K., Carlsson, M., Svensson, L. A., and Liljas, A. (1992) Structure of native and apo carbonic anhydrase II and structure of some of its anion-ligand complexes. *J. Mol. Biol. 227*, 1192–1204.
7. Liang, J. Y., and Lipscomb, W. N. (1990) Binding of substrate $CO_2$ to the active site of human carbonic anhydrase II: A molecular dynamics study. *Proc. Natl. Acad. Sci. U.S.A. 87*, 3675–3679.
8. Lindskog, S. (1997) Structure and mechanism of carbonic anhydrase. *Pharmacol. Ther. 74*, 1–20.
9. Tu, C. K., Silverman, D. N., Forsman, C., Jonsson, B.-H., and Lindskog, S. (1989) Role of histidine 64 in the catalytic mechanism of human carbonic anhydrase II studies with a site-specific mutant. *Biochemistry 28*, 7913–7918.
10. Nair, S. K., and Christianson, D. W. (1991) Unexpected pH-dependent conformation of His64, the proton shuttle of carbonic anhydrase II. *J. Am. Chem. Soc. 113*, 9455–9458.
11. Fisher, S. Z., Hernandez-Prada, J., Tu, C. K., Duda, D., Yoshioka, C., An, H., Govindasamy, L., Silverman, D. N., and McKenna, R. (2005) Structural and kinetic characterization of active-site histidine as a proton shuttle in catalysis by human carbonic anhydrase II. *Biochemistry 44*, 1097–1105.
12. De Grotthuss, C. J. T. (1806) Memoir on the decomposition of water and of the bodies that it holds in solution by means of galvanic electricity. *Ann. Chim. 58*, 54–73.
13. Maupin, C. M., McKenna, R., Silverman, D. N., and Voth, G. A. (2009) Elucidation of the proton transport mechanism in human carbonic anhydrase II. *J. Am. Chem. Soc. 131*, 7598–7608.
14. Riccardi, D., Konig, P., Guo, H., and Cui, Q. (2008) Proton transfer in carbonic anhydrase is controlled by electrostatics rather than the orientation of the acceptor. *Biochemistry 47*, 2369–2378.
15. Roy, A., and Taraphder, S. (2007) Identification of proton-transfer pathways in human carbonic anhydrase II. *J. Phys. Chem. B 111*, 10563–10576.
16. Fisher, S. Z., Tu, C. K., Bhatt, D., Govindasamy, L., Agbandje-McKenna, M., McKenna, R., and Silverman, D. N. (2007) Speeding up proton transfer in a fast enzyme: Kinetic and crystallographic studies on the effect of hydrophobic amino acids substitutions in the active site of human carbonic anhydrase II. *Biochemistry 46*, 3803–3813.
17. Duda, D., Govindasamy, L., Agbandje-McKenna, M., Tu, C., Silverman, D. N., and McKenna, R. (2003) The refined atomic structure of carbonic anhydrase II at 1.05 Å resolution: Implications of chemical rescue of proton transfer. *Acta Crystallogr. D59*, 93–104.
18. Fisher, S. Z., Maupin, C. M., Budayova-Spano, M., Govindasamy, L., Tu, C. K., Agbandje-McKenna, M., Silverman, D. N., Voth,

G. A., and McKenna, R. (2007) Atomic crystal and molecular dynamics simulation structures of human carbonic anhydrase II: Insights into the proton transfer mechanism. *Biochemistry 46*, 2930–2937.
19. Meilleur, F., Myles, D. A. A., and Blakeley, M. P. (2006) Neutron Laue macromolecular crystallography. *Eur. Biophys. J. 35*, 611–620.
20. Shu, F., Ramakrishnan, V., and Schoenborn, B. P. (2000) Enhanced visibility of hydrogen atoms by neutron crystallography on fully deuterated myoglobin. *Proc. Natl. Acad. Sci. U.S.A. 97*, 3872–3877.
21. Adams, P. D., Mustyakimov, M., Afonine, P. V., and Langan, P. (2009) Generalized X-ray and neutron crystallographic analysis: More accurate and complete structure for biological macromolecules. *Acta Crystallogr. D65*, 567–573.
22. Kovalevsky, A., Katz, A., Carrel, H. L., Hanson, L., Mustyakimov, M., Fisher, S. Z., Coates, L., Schoenborn, B. P., Bunick, G. J., Glusker, J., and Langan, P. (2008) Hydrogen location in stages of an enzyme-catalyzed reaction: Time-of-flight neutron structure of D-xylose isomerase with bound D-xylulose. *Biochemistry 47*, 7595–7597.
23. Blum, M. M., Mustyakimov, M., Ruterjans, H., Kehe, K., Schoenborn, B. P., Langan, P., and Chen, J. C. (2009) Rapid determination of hydrogen positions and protonation states of diisopropyl fluorophosphatase by joint neutron and X-ray diffraction refinement. *Proc. Natl. Acad. Sci. U.S.A. 106*, 713–718.
24. Fisher, S. Z., Kovalevsky, A., Domsic, J., Mustyakimov, M., Silverman, D. N., McKenna, R., and Langan, P. (2009) Preliminary joint neutron and X-ray crystallographic study of human carbonic anhydrase II. *Acta Crystallogr. F65*, 495–498.
25. Langan, P., Fisher, S. Z., Kovalevsky, A., Mustyakimov, M., Sutcliffe Valone, A., Unkefer, C., Waltman, M. J., Coates, L., Adams, P. D., Afonine, P. V., Bennett, B., Dealwis, C., and Schoenborn, B. P. (2008) Protein structures by spallation neutron crystallography. *J. Synchrotron Radiat. 15*, 215–218.
26. Schoenborn, B. P., and Langan, P. (2004) Protein crystallography with spallation neutrons. *J. Synchrotron Radiat. 11*, 80–82.
27. Helliwell, J. R., Habash, J., Cruickshank, D. W. J., Harding, M. M., Greenhough, T. J., Campbell, J. W., Clifton, I. J., Elder, M., Machin, P. A., Papiz, M. Z., and Zurek, S. (1989) The recording and analysis of synchrotron X-radiation Laue diffraction photographs. *J. Appl. Crystallogr. 22*, 483–497.
28. Collaborative Computational Project, Number 4 (1994) *Acta Crystallogr. D50*, 760–763.
29. Otwinowski, Z., and Minor, W. (1997) Processing of X-ray diffraction data collected in oscillation mode. *Methods Enzymol. 276*, 307–326.
30. Brünger, A. T., Adams, P. D., Clore, G. M., DeLano, W. L., Gros, P., Grosse-Kunstleve, R. W., Jiang, J.-S., Kuszewski, J., Nilges, M., Pannu, N. S., Read, R. J., Rice, Simonson, T., and Warren, G. L. (1998) Crystallography and NMR system: A new software suite for macromolecular structure determination. *Acta Crystallogr. D54*, 905–921.
31. Sheldrick, G. M. (2008) A short history of SHELX. *Acta Crystallogr. A64*, 112–122.
32. Emsley, P., and Cowtan, K. (2004) Coot: Model-building tools for molecular graphics. *Acta Crystallogr. D60*, 2126–2132.
33. DeLano, W. L. (2002) The PyMOL Molecular Graphics System, DeLano Scientific, San Carlos, CA. http://www.pymol.org.
34. Orpen, A. G., Brammer, L., Allen, F. H., Kennard, O., Watson, D. G., and Taylor, R. (1989) *J. Chem. Soc., Dalton Trans.* No. Suppl., 1–83.
35. Schowen, K. B., and Schowen, R. L. (1982) Solvent isotope effects of enzyme systems. *Methods Enzymol. 87*, 551–606.
36. Avvaru, B., Arenas, D. J., Tu, C. K., Tanner, D. B., McKenna, R., and Silverman, D. N. (2009) Spectroscopic and crystallographic studies Co(II)-substituted human carbonic anhydrase II. *Biochemistry* h (submitted for publication).
37. Avvaru, B., Kim, C. U., Sippel, K., Gruner, S., Agbandje-McKenna, M., Silverman, D. N., and McKenna, R. (2009) A short, strong hydrogen bond in the active site of human carbonic anhydrase II. *Biochemistry* (in press).
38. Merz, K. M. (1990) Insights into the function of the zinc-hydroxide Thr199-Glu106 hydrogen bonding network in carbonic anhydrases. *J. Mol. Biol. 214*, 799–802.
39. Jeans, C., Schilstra, M. J., Ray, N., Husain, S., Minagawa, J., Nugent, J. H. A., and Klug, D. R. (2002) Replacement of tyrosine D with phenylalanine affects the normal proton transfer pathways for the reduction of $P680^+$ in oxygen-evolving photosystem II particles from *Chlamydomonas*. *Biochemistry 41*, 15754–15761.
40. Pival, S. L., Klimacek, M., Kratzer, R., and Nidetzky, B. (2008) Tyr51 is the proton donor-acceptor for NAD(H)-dependent interconversion of xylose and xylitol by *Candida tenuis* xylose reductase (AKR2B5). *FEBS Lett. 582*, 4095–4099.